Earth, Planets and Space

FULL PAPER

Wire Probe Antenna (WPT) and Electric Field Detector (EFD) of Plasma Wave Experiment (PWE) aboard the Arase satellite: specifications and initial evaluation results

Yasumasa Kasaba[1*] , Keigo Ishisaka[2], Yoshiya Kasahara[3], Tomohiko Imachi[3], Satoshi Yagitani[3], Hirotsugu Kojima[4], Shoya Matsuda[5], Masafumi Shoji[5], Satoshi Kurita[5], Tomoaki Hori[5], Atsuki Shinbori[5], Mariko Teramoto[5], Yoshizumi Miyoshi[5], Tomoko Nakagawa[6], Naoko Takahashi[7], Yukitoshi Nishimura[8,9], Ayako Matsuoka[10], Atsushi Kumamoto[1], Fuminori Tsuchiya[11] and Reiko Nomura[12]

Abstract

This paper summarizes the specifications and initial evaluation results of Wire Probe Antenna (WPT) and Electric Field Detector (EFD), the key components for the electric field measurement of the Plasma Wave Experiment (PWE) aboard the Arase (ERG) satellite. WPT consists of two pairs of dipole antennas with ~ 31-m tip-to-tip length. Each antenna element has a spherical probe (60 mm diameter) at each end of the wire (15 m length). They are extended orthogonally in the spin plane of the spacecraft, which is roughly perpendicular to the Sun and enables to measure the electric field in the frequency range of DC to 10 MHz. This system is almost identical to the WPT of Plasma Wave Investigation aboard the BepiColombo Mercury Magnetospheric Orbiter, except for the material of the spherical probe (ERG: Al alloy, MMO: Ti alloy). EFD is a part of the EWO (EFD/WFC/OFA) receiver and measures the 2-ch electric field at a sampling rate of 512 Hz (dynamic range: ± 200 mV/m) and the 4-ch spacecraft potential at a sampling rate of 128 Hz (dynamic range: ± 100 V and ± 3 V/m), with the bias control capability of WPT. The electric field waveform provides (1) fundamental information about the plasma dynamics and accelerations and (2) the characteristics of MHD and ion waves in various magnetospheric statuses with the magnetic field measured by MGF and PWE–MSC. The spacecraft potential provides information on thermal electron plasma variations and structure combined with the electron density obtained from the upper hybrid resonance frequency provided by PWE–HFA. EFD has two data modes. The continuous (medium-mode) data are provided as (1) 2-ch waveforms at 64 Hz (in apoapsis mode, $L > 4$) or 256 Hz (in periapsis mode, $L < 4$), (2) 1-ch spectrum within 1–232 Hz with 1-s resolution, and (3) 4-ch spacecraft potential at 8 Hz. The burst (high-mode) data are intermittently obtained as (4) 2-ch waveforms at 512 Hz and (5) 4-ch spacecraft potential at 128 Hz and downloaded with the WFC-E/B datasets after the selection. This paper also shows the initial evaluation results in the initial observation phase.

Keywords: Electric field, Plasma wave, Spacecraft potential, Electron density and temperature, Wire Probe Antenna (WPT), Electric Field Detector (EFD), Plasma Wave Experiment (PWE), Arase spacecraft

*Correspondence: kasaba@pat.gp.tohoku.ac.jp
[1] Department of Geophysics, Tohoku University, Aoba-ku, Sendai, Miyagi 980-8578, Japan
Full list of author information is available at the end of the article

Kasaba *et al. Earth, Planets and Space* (2017) 69:174

Page 2 of 18

Introduction

The Arase/ERG (Exploration of energization and Radiation in Geospace) project is a mission to study the acceleration and loss mechanisms of relativistic electrons around the Earth (Miyoshi et al. 2012, 2017a, b). The spacecraft was successfully launched on December 20, 2016, and started exploring the heart of the Earth's radiation belt using electromagnetic field instruments covering a wide frequency range and charged particle detectors over a wide energy range.

The Plasma Wave Experiment (PWE) was developed as one of the key instruments for this project, in order to observe electric fields, plasma waves, and radio waves in geospace (Kasahara et al. 2016). An electric field provides information about plasma transports and accelerations and plays an important role in controlling the global dynamics of the inner magnetosphere. Plasma waves provide the characteristics and strength of nonlinear energy and momentum exchanges and enable us to study the processes of high-energy particle accelerations. Plasma waves such as whistler mode chorus, electromagnetic ion cyclotron wave, and magnetosonic wave interact with plasma over a wide energy range and consequently contribute to loss and acceleration processes of high-energy particles in geospace. Radio waves can be used as remote-sensing tools of auroral and magnetospheric activities such as auroral kilometric and continuum radiations. PWE provides electron density information from the upper hybrid resonance (UHR) frequency. Spacecraft potential from PWE also includes information about both electron temperature and density. By those data, PWE is expected to provide key information about the structure, dynamics, and physical processes governing the geospace, through collaborations with other instruments aboard Arase and multiple spacecraft flying in the inner magnetosphere.

To meet the above-mentioned scientific objectives, PWE uses two sets of orthogonal electric field sensors (WPT; Wire Probe Antennas) and three-axis magnetic sensors (MSC; Magnetic Search Coil). Their signals are served to three receivers, named EFD (Electric Field Detector) covering less than ~ 100 Hz in electric field; WFC/OFA (WaveForm Capture and Onboard Frequency Analyzer) covering from 10 Hz to 20 kHz in both electric and magnetic fields; and HFA (High-Frequency Analyzer) covering from 10 to 10 MHz in electric field and from 10 to 100 kHz in magnetic field. Descriptions of PWE, including its design and specifications, are detailed in Kasahara et al. (2017) for overall PWE and EWO (and WFC/OFA), Kumamoto et al. (2017) for HFA, Ozaki et al. (2017) for MSC, and Matsuda et al. (2017) for onboard data processing.

This paper summarizes the specifications and initial evaluation results of the WPT and EFD systems. Figure 1

shows the block diagram of WPT and EFD in the PWE system. WPT consists of four wire antenna booms (WPT Sensor; WPT-S) and their preamplifiers (WPT Preamplifier; WPT-Pre) and forms two orthogonal pairs of dipole antennas with ~ 31-m tip-to-tip length. The output signals of WPT-Pre are served to three electric field receivers, EFD, WFC/OFA-E, and HFA, in the PWE main electrical box (PWE-E). EFD forms a part of the EWO (EFD/WFC/OFA) receiver and measures the 2-ch differential electric field at 512 Hz and 4-ch spacecraft potential at 128 Hz. It also feeds the bias current to WPT. The output of EFD is processed on the PWE CPU#8 unit and converted to the telemetry to the ground. PWE-E also contains the MAST (extendable mast) and WPT deployment control Electronics (MWE).

Through the combination of WPT and EFD, PWE can investigate an electric field waveform as (1) the fundamental information of the plasma dynamics and accelerations and (2) the characteristics of MHD and ion waves, including their Poynting vectors in the inner magnetosphere, in combination with the magnetic field measurement by MGF and PWE–MSC. PWE can also provide spacecraft potential as the diagnostics for thermal electron plasma variations and structure, supported by the electron density from the UHR frequency provided by PWE–HFA and low-energy particle measurements.

The specification and the development team of these units are summarized in Table 1. On the Van Allen Probes which have flown in the Geospace before Arase's launch, the EFW instrument (Wygant et al. 2013) intensively observed the electric field. EFW can measure three-dimensional electric fields using two pairs of spherical dipole probes in the spin plane with 100-m tip-to-tip length and one pair of spin-axis dipole antenna with 15-m tip-to-tip length. Although Arase PWE has only two-dimensional electric fields using the pair of shorter dipole antenna, we will establish the good collaborative sciences together, not only with them but also with EFI aboard the THEMIS probes (Bonnell et al. 2008) and FIELD aboard the MMS probes (Torbert et al. 2016). This paper shows the specifications of WPT ["Wire Probe Antenna (WPT)" section] and EFD ["Electric Field Detector (EFD) in EWO (EFD-WFC-OFA)" section], onboard data scheme (Onboard data processing and data pipeline on the ground" section), and the initial operation and evaluation results ("Initial evaluation status" section).

Wire Probe Antenna (WPT)

Wpt-s

The WPT system comprises two pairs of spherical double-probe sensors at the ends of booms orthogonally deployed in the spin plane, designed on the heritage of the Geotail PANT system, which is connected to two
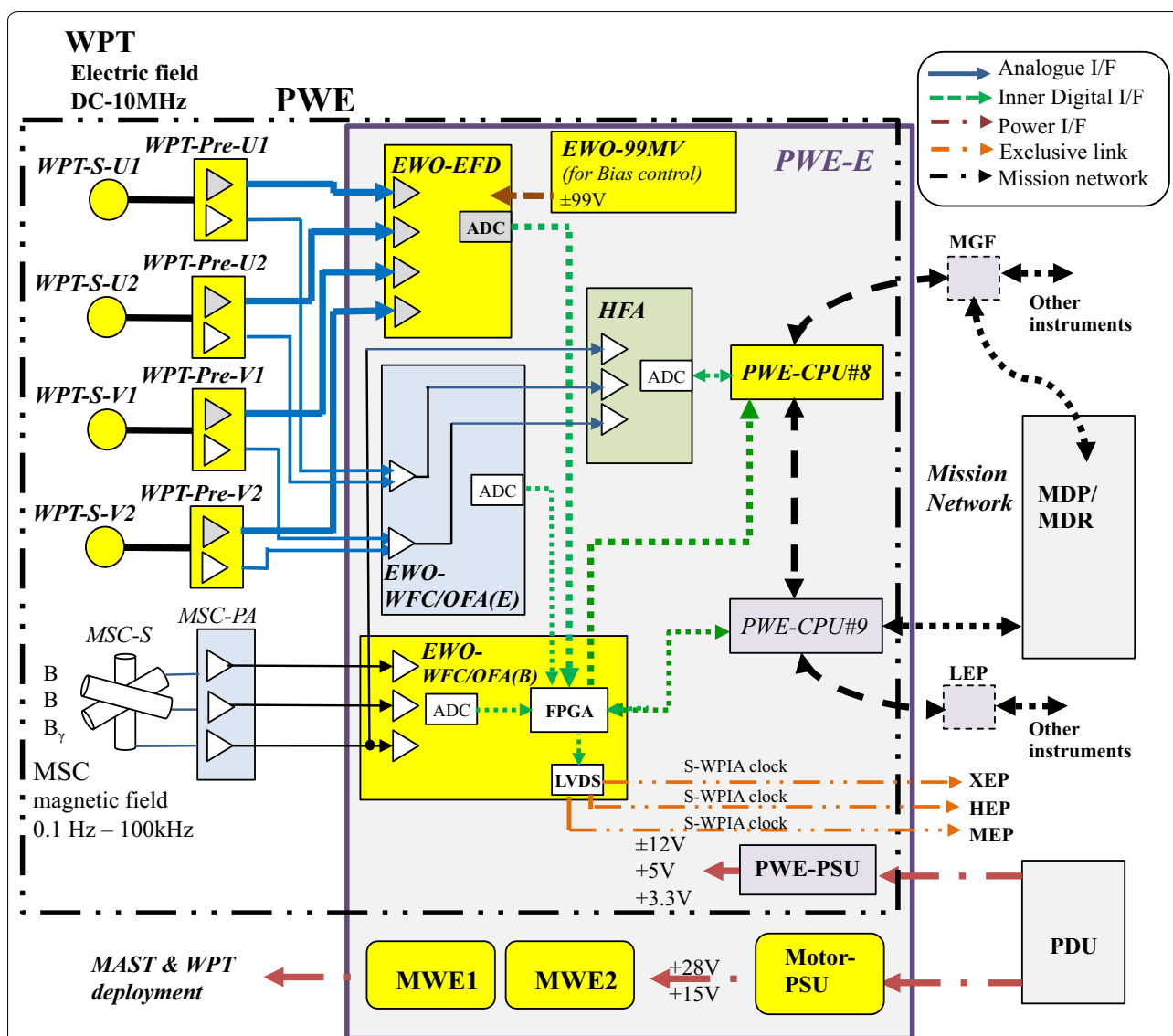
Kasaba *et al. Earth, Planets and Space* (2017) 69:174

Page 3 of 18

Fig. 1 Block diagram of the PWE and related systems aboard the Arase spacecraft. This paper deals with the WPT and EFD systems (yellow parts) in the PWE. [Modified from Fig. 2 of Kasahara et al. (2017)]

Table 1 Specification and the provisional teams of the WPT-S and EFD systems

		Properties	Resource	Provided from
WPT	WPT-S_1-4	Wire antennas (15-m) and their preamps (< 10 MHz in E-field)	0.80 kg ×4	Nippi Corporation Y. Kasaba (Tohoku Univ.) et al.
	WPT-Pre_1-4		0.18 kg ×4	Mitsubishi Heavy Industries H. Kojima (Kyoto Univ.) et al.
PWE-E			6.33 kg in total	Mitsubishi Heavy Industries H. Kojima (Kyoto Univ.) et al.
	EFD (a part of EWO)	Low-frequency E-field receiver (< 224 Hz) with spacecraft potential	0.73 kg (EWO)	Mitsubishi Heavy Industries Y. Kasaba (Kyoto Univ.) et al.
	MV99 V	± 99 V power supply for EFD bias control	0.10 kg	Meisei Electric Co. Y. Kasaba (Tohoku Univ.) et al.
	MWE_1-2	Deployment controller for MAST and WPT-S	0.45 kg 0.42 kg	Nippi Corporation A. Matsuoka (ISAS/JAXA) et al.

Kasaba *et al. Earth, Planets and Space* (2017) 69:174

Page 4 of 18

receivers: EFD for DC electric field (Tsuruda et al. 1994) and the Plasma Wave Instrument (PWI) for plasma and radio waves (Matsumoto et al. 1994). The PANT system comprises a pair of a 50-m-long wire antenna (tip-to-tip length: 102 m) and a 100-mm-diameter sphere on its top. Ideally, the wire probes should be longer than the local Debye length. However, the practical length is limited due to technical feasibilities. To reduce the technical risks and development costs, the Arase WPT system was made almost identical to the WPT system of the PWI aboard the BepiColombo Mercury Magnetospheric Orbiter (Kasaba et al. 2010). Therefore, the wire length of 15 m (tip-to-tip length: 31 m) and sphere diameter of 60 mm are common to those of BepiColombo/MMO PWI. The difference lies in the material of the spherical probe, which was changed from titanium alloy (MMO) to aluminum alloy (Arase) for the reduction in the sphere mass. (MMO needs to endure in higher-temperature range.)
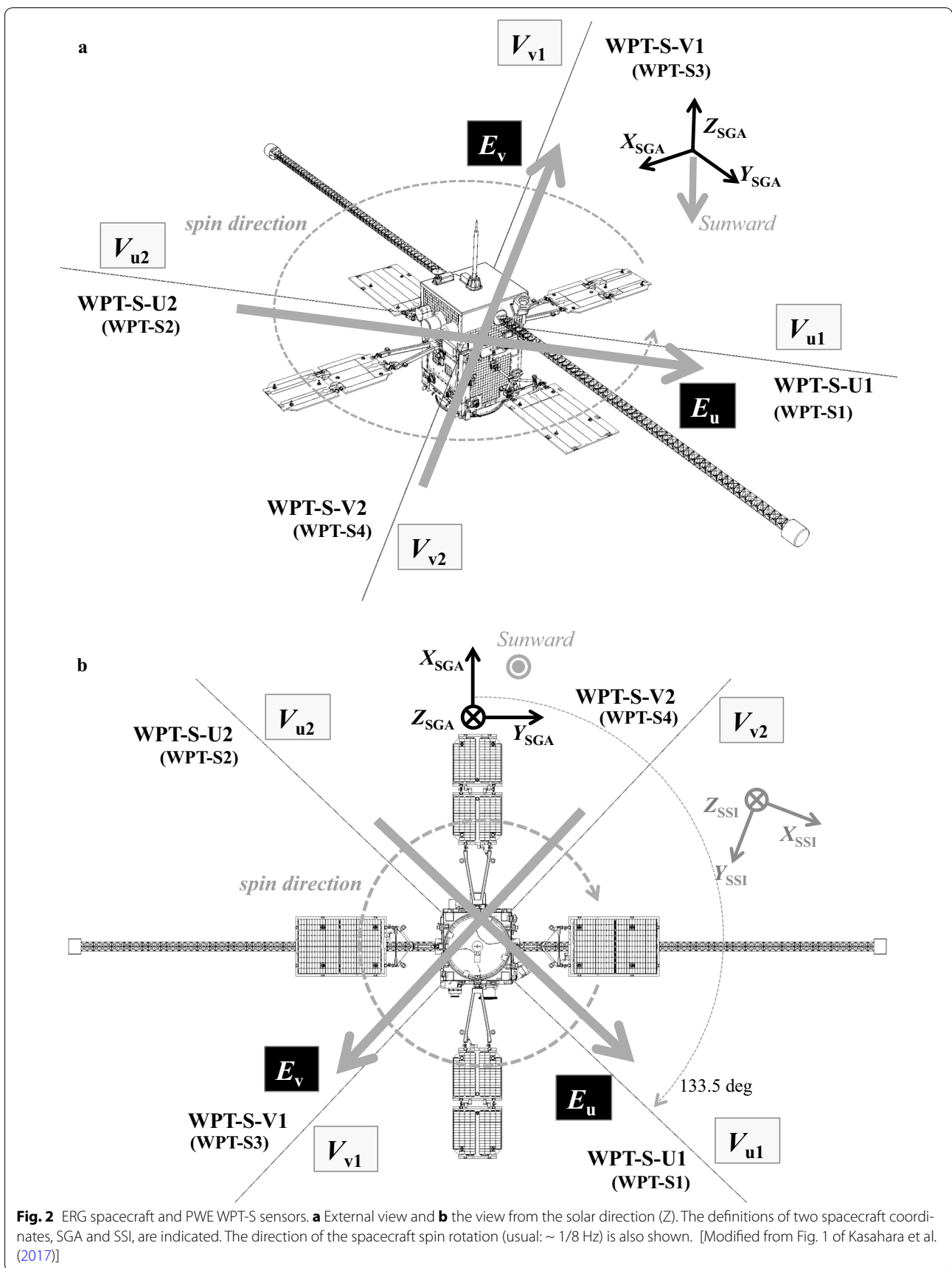
Four WPT-S wire booms, WPT-S-U1, WPT-S-U2, WPT-S-V1, and WPT-S-V2, are orthogonally installed on Arase's spin plane. Figure 2 describes their geometry in (a) the external view and (b) the view from the Z-axis (spin axis), with the definition of Arase's coordinates. The angle of WPT-S-U1 from the spacecraft X-axis is $+ 133.5°$ in the Spinning Satellite Geometry Axis coordinate and $+ 21.9°$ in the Spinning Sun sensor Inertia (SSI) coordinate. In both coordinates, Arase's spin axis is parallel to the Z-axis, and "$- Z$" is set to sunward. The difference from the solar direction is controlled around 15° (at most, within 4–20°). Therefore, a large variation in photoelectron flux associated with the spacecraft spin motion is not expected.
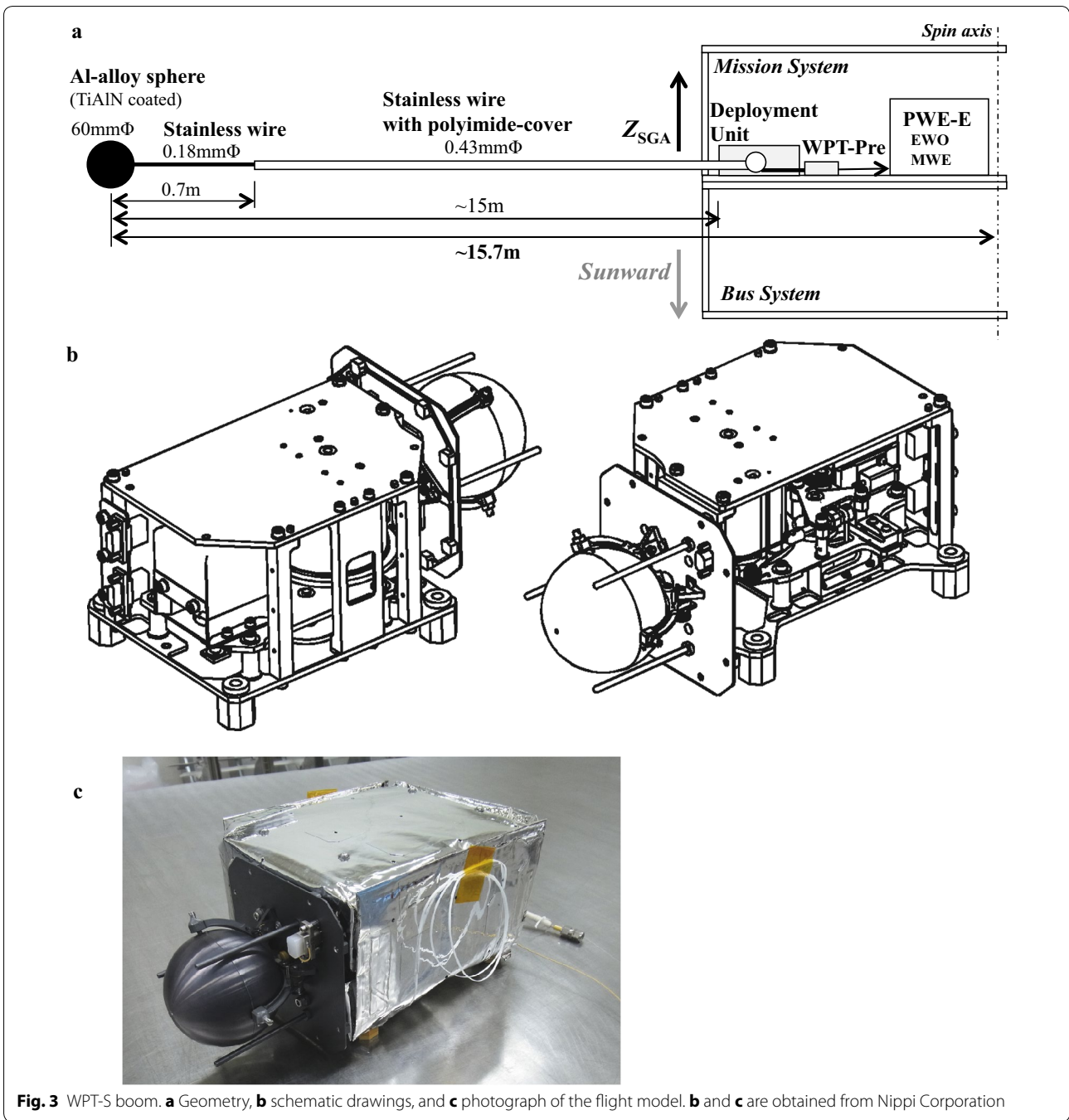
Figure 3 shows (a) the geometry, (b) schematic drawings, and (c) a photograph of the WPT-S sensor. The deployment units are installed at ~ 0.6 m from the spacecraft spin axis. After the full deployment, four WPT wire booms form the two-dipole antenna with ~ 31-m tip-to-tip length. (The distances of WPT-S booms from the spacecraft spin axis are slightly different. The precise tip-to-tip length is 31.22 m for WPT-S U pairs and 31.30 m for WPT-S V pairs.)

As described above, the basic geometry is similar to that of BepiColombo/MMO PWI/WPT-S. Each wire boom is composed of a 15-m-long conductive wire and a 60-mm-diameter sphere on its top. The conductive wire is made of stainless steel (SUS316L, diameter: 0.18 mm) and covered by a polyimide insulator (diameter: 0.43 mm) except a 0.7-m-long top-side area, which is coated by Aerodag (a graphite paint). The sphere is an Al alloy (7075-T7351) shell with thickness of less than 1 mm attached to the tip of the conductive wire. In this configuration, the conductive top part, i.e., the 60-mm-diameter

sphere and the 0.7-m-long conductive wire (its cross section: less than 5% of the sphere's), become the probe for contact with ambient plasma. Such surfaces are preferred to have uniform conductivity, photoelectron emissivity, and secondary photoelectron yield. The sphere surface, which has a much larger area than that of the conductive wire part, is coated with TiAlN with a Ti:Al ratio of 2:1 and thickness of ~ 1 μm, as the spherical probe of MMO PWI WPT-S. As the prelaunch test, the nonuniformity of the photoelectron emissivity under the illumination of a deuterium lamp was evaluated using a vacuum chamber with the help of Prof. Kobayashi (Saitama University). In this study, the photoelectron emission from the vacuum ultraviolet light is observed using an electron emission microscope (EEM) (Suharyanto et al. 2006). The sputtered TiAlN and TiN surface exhibits a nonuniformity of 1.2%, whereas the reference surface, which is a baked carbon coating (baked Aerodag) used in the Geotail PANT spheres, exhibits a nonuniformity of 2.0%. The evaluation of the performance and degradation of TiAlN in space is one of the objectives for Arase's WPT, as the pretest of BepiColombo's WPT. The conductive part of the wire's top-side area limits the influence of the surface potential of the insulated part on the top sphere. The remaining surface area, covered with polyimide, limits the coupling of the long conductive wire to ambient plasma. Inside of the deployment unit, the wire is covered with a copper-meshed shield (diameter: 0.61 mm).

For DC and low-frequency electric field at a frequency of less than several 10 s Hz, the WPT-S sensor part couples with plasma in its top area, i.e., the sphere and the conductive part of the wire. The effective length is expected to be of the same order as the tip-to-tip length, i.e., ~ 30 m. To sense the potential difference between two probes, the principle of the double-probe electric field measurement is kept identical to that of a voltmeter. The floating potential of a conductive material in space plasma is roughly determined by the balance between the outflow photoelectrons and inflow ambient electrons. In thin plasma with a density of $< ~ 100$ cm^{-3} (outside of the plasmapause), the inflow photoelectron current, I_{ph} (few nA/cm^2, few 10 s nA), is much larger than the outflow ambient electron current, I_e (< 1 nA/cm^2, < 10 nA). In sunlight, the probe potential becomes much higher than the potential of ambient plasma. Under this "floating" condition, the resistance of the probe to ambient plasma is larger than several 100 MΩ, and the probe potential varies considerably with ambient electron density and temperature. To reduce this resistance and stabilize the probe potential close to that of ambient plasma, we feed a bias current, I_b, to the probe in the order of few 10 s nA, less than the amount of the outflow photocurrent, in order to use the region close to the highest gradient of

Kasaba *et al. Earth, Planets and Space* (2017) 69:174

Page 5 of 18

Fig. 2 ERG spacecraft and PWE WPT-S sensors. **a** External view and **b** the view from the solar direction (Z). The definitions of two spacecraft coordinates, SGA and SSI, are indicated. The direction of the spacecraft spin rotation (usual: ~ 1/8 Hz) is also shown. [Modified from Fig. 1 of Kasahara et al. (2017)]

Kasaba *et al. Earth, Planets and Space* (2017) 69:174

Page 6 of 18

Fig. 3 WPT-S boom. **a** Geometry, **b** schematic drawings, and **c** photograph of the flight model. **b** and **c** are obtained from Nippi Corporation

the photoelectron current to the S/C potential (i.e., lowest impedance) (Pedersen et al. 1998). Using the biased probe, the resistance to ambient plasma becomes several MΩ to ∼ 100 MΩ. It also enables us to use "spacecraft potential" as an indicator of the surrounding electron density and temperature, which supports other electron density measurements, i.e., UHR frequency measurement by PWE–HFA and low-energy particle measurement by particle instruments.

In the frequency range of more than several 10 s Hz, WPT-S acts as a pair of dipole wire antennas with a length of ∼ 31 m (effective length: ∼ 15.5 m) or four monopole antennas, each ∼ 15.5 m long. The antenna capacity C_{ant} in vacuum can be expressed as:

$$C_{ant} = C_{wire} + C_{sphere} = \frac{l}{120c \ln{(2l/a)}} + 4\pi\varepsilon_0 R \quad (1)$$

Kasaba *et al. Earth, Planets and Space* (2017) 69:174

Page 7 of 18

where C_{wire} is the capacitance of the wire, c is the speed of light, l is the length of the wire (15 m), a is the radius of the wire (0.18 mm), C_{sphere} is the capacitance of the sphere, ε_0 is the electric permittivity in vacuum, and R is the radius of the sphere (30 mm). For each monopole antenna, C_{wire} and C_{sphere} for a single probe are expected to be 35 and 3.4 pF, respectively. In real space, plasma sheath impedance is also taken into account.

The deployment unit consists of two parts: a sphere holder and a motor box. The sphere holder keeps the sphere using a launch lock with three latching arms. The motor box contains a wire holder, a stepping motor, a gear box, and a latch-release mechanism, and is driven by MWE (MAST-WPT-E, MAST, and WPT Electronics) in PWE-E. As the first step of the deployment operation, the launch lock is released by the initial rotation of the wire holder driven by the stepping motor. Next, the wire is deployed in three steps, i.e., 5, 10 m, and full (15 m).

WPT-Pre (WPT preamplifier)

Four WPT-Preamplifiers (WPT-Pre-U1, WPT-Pre-U2, WPT-Pre-V1, and WPT-Pre-V2) are installed at the side of, and connected to, the corresponding WPT booms (WPT-S-U1, WPT-S-U2, WPT-S-V1, and WPT-S-V2).

To cover the frequency range from DC to 10 MHz in the spacecraft potential within ± 100 V, WPT-Pre consists of two amplifiers: WPT-Pre (DC) and WPT-pre (AC) (Fig. 4); this design is similar to that of BepiColombo/ MMO PWI/WPT-Pre.

WPT-Pre (DC) covers the signals at lower frequencies from DC to ~ 200 Hz, with a wider dynamic range and lower sensitivity. It is connected to WPT-S through a voltage-divider circuit (10 GΩ (with 1 pF) and 1 GΩ (with 10 pF)), with a gain of − 20 dB. Its output signal is fed to the EWO-EFD receiver. The dynamic range of WPT-Pre (DC) is ± 100 V. EWO-EFD comprises a bias feedback path through the bias register (100 MΩ), in order to maintain high input impedance by bootstrapping and to feed the bias current to the probe. This register can be switched to the calibration register (1 MΩ). The radiation dose level of the active parts (OP15) is limited to below 50 krad with its chassis thickness and tantalum point shield. The output signal is directly fed to EWO-EFD.

WPT-Pre (AC) covers the frequency range from 10 Hz to 10 MHz. Its input is isolated from WPT-Pre (DC) by a 220-pF capacitance and decouples the spacecraft potential with few V to few 10 s V and the spin modulation of
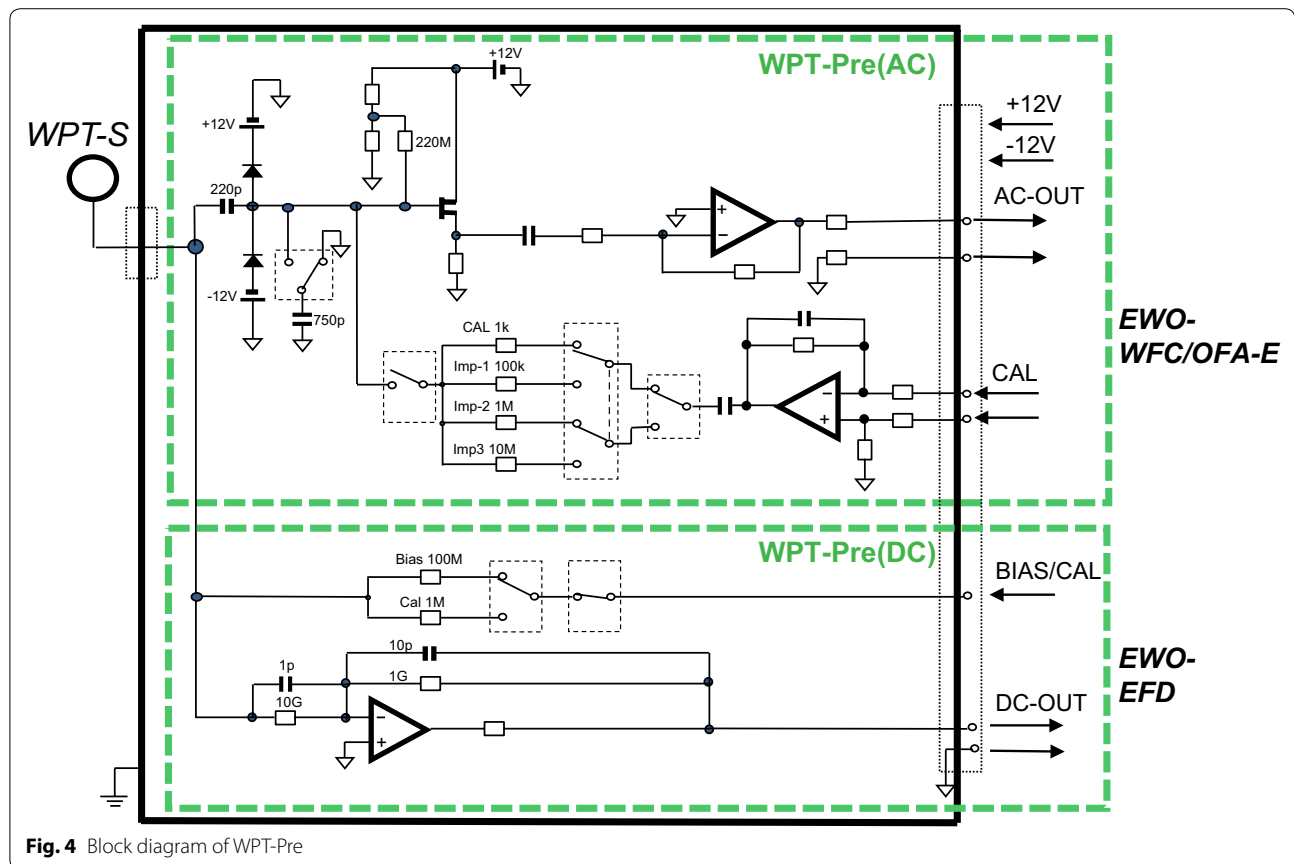

Fig. 4 Block diagram of WPT-Pre

Kasaba *et al. Earth, Planets and Space* (2017) 69:174

Page 8 of 18

the DC electric field with few mV/m to few 100 s mV/m (Arase's spin rate: ~ 1/8 Hz). The gain of WPT-Pre (AC) is set to ~ 6 dB (high-gain mode) and compensates for the loss at the connection of WPT-S and WPT-Pre (AC). The capability to measure large whistler waves with intensities of more than a few tens of mV/m is provided by an input attenuator and a capacitance of 750 pF (low-gain mode). The attenuation level is decided in relation to the antenna impedance and this 750-pF capacitance. If we assume the typical antenna impedance in vacuum, the expected attenuation level is ~ − 20 dB. Actually, the antenna impedance depends on the local plasma density and its temperature. The antenna impedance can be evaluated using the onboard antenna impedance measurement system, conducted by changing the calibration resistances (1 kΩ, 100 kΩ, 1 MΩ, and 10 MΩ) with the calibration signal from the EWO source clock (Kasahara et al. 2017; Matsuda et al. 2017). Since the low-gain mode can also affect the input impedance of WPT-Pre (DC), the gain and phase curve of WPT-Pre (DC) and EFD are

also affected; this is shown in "Electric Field Detector (EFD) in EWO (EFD-WFC-OFA)" in section. (We have not yet used the low-gain mode as of August 2017). The output signal of WPT-Pre (AC) is fed to EWO-WFC/OFA (E), and HFA receives the signal through WFC/OFA (E).

Electric Field Detector (EFD) in EWO (EFD-WFC-OFA)

The PWE system shown in Fig. 1 consists of three receiver components: EWO (EFD, WFC, and OFA) and HFA. These are installed into a single chassis, called PWE-E, and receive electric field signals from the four WPT-Pres and magnetic field signals from the three-axis MSC on the MAST boom.

The block diagram of EFD is shown in Fig. 5. This design is similar to that of BepiColombo/MMO PWI/WPT-EFD, except for the gain and filter frequency settings. EFD is a 2-ch EWO receiver unit covering the low-frequency electric field part and is dedicated to
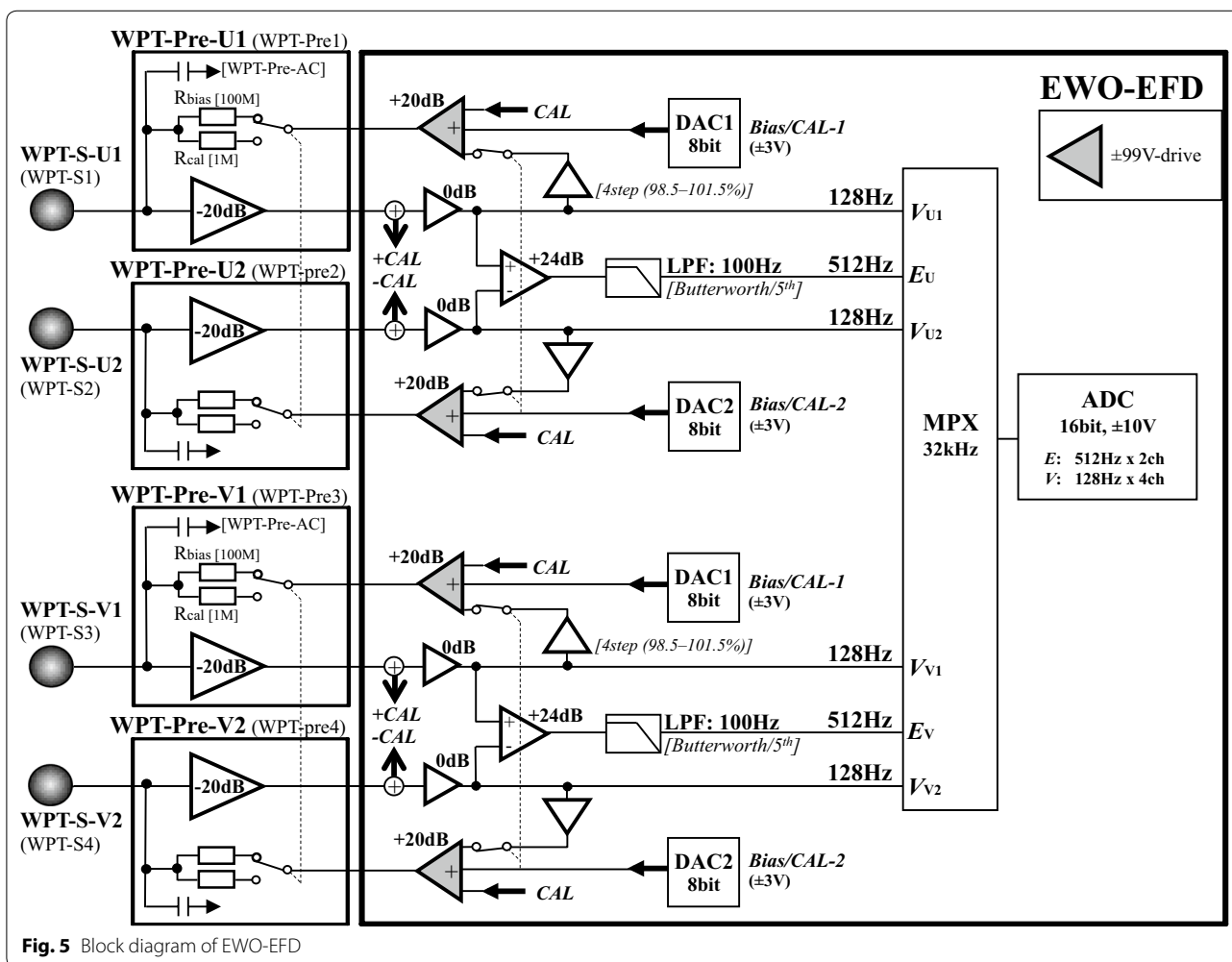

Fig. 5 Block diagram of EWO-EFD

Kasaba *et al. Earth, Planets and Space* (2017) 69:174

Page 9 of 18

observation of frequencies ranging from DC to ~ 100 Hz. It provides two types of outputs, as summarized in Table 2. (1) 2-ch electric field waveform in the spin plane, as the differential voltage between the U1/U2 (E_u component) and V1/V2 pairs (E_v component). Both signals are simultaneously digitized (resolution: 16 bit) at a sampling rate of 512 Hz after passing through the low-pass filter with a cutoff frequency of 100 Hz (the fifth Butterworth filter, − 30 dB/octave, − 100 dB/decade). With the dynamic range of ± 10 V at the ADC and the gain of + 4 dB from WPT-Pre (DC) and EFD, the saturation level for the electric field measurement is ~ ± 200 mV/m with a resolution of ~ 0.006 mV/m, if the dipole antenna has an effective length of ~ 30 m. (2) 4-ch spacecraft potential voltage of WPT-S-U1 (V_{u1}), WPT-S-U2 (V_{u2}), WPT-S-V1 (V_{v1}), and WPT-S-V2 (V_{v2}). These signals are not simultaneously digitized (with the difference of ~ 1-ms resolution: 16 bit) at the sampling rate of 128 Hz. With the dynamic range of 0–10 V at the ADC and the gain of − 20 dB from WPT-Pre (DC) (without the low-pass filter), the saturation level is ± 100 V with a resolution of 3 mV.

EFD serves the bias current control capability for the WPT system, which can be set within ± 300 nA in 256 steps (resolution: 2.34 nA) through the bias register (100 MΩ), from the bias feedback amplifier driven by the ± 99 V power supply (MV99 V). In the initial operation from March 2017, ~ 19 nA was constantly fed as the bias current to all probes. By the bootstrapping of this feedback loop through EFD's bias amplifier with a gain of ~ 0.99, the effective input impedance of WPT-Pre (DC) can exceed 1 GΩ. Such high impedance is sufficiently larger than the plasma resistance to ambient plasma and enables us to appropriately measure the space plasma potential. The bias current circuit is also used for two calibration signals: (1) The bias current sweep mode, in which the bias current is changed within ± 300 nA during 0.5 s, in order to evaluate the antenna resistance measurement through the evaluation of Langmuir curve as the relation between bias current and probe potential. (2) The voltage calibration mode, in which the bias circuit serves the fixed voltage to the WPT-Pre input through the calibration register (1 MΩ), within the dynamic range of ± 30 V in 256 steps under the disconnection of the loop-back route in the bias amplifier in EWO-EFD.

In both cases, the amount of bias current (or calibration signals) can be set separately for the U1/V1 and U2/V2 pairs. (U1/V1 cannot set different values and U2/V2 is same. This restriction is caused by the restrictions of the design from that of MMO PWI/EWO-EFD; MMO PWI has only one WPT-S pair).

Figure 6 shows the expected gain and phase characteristics of the WPT-Pre (DC) and EFD systems, with the expected input load at WPT-S. Actually, the gain, phase, and phase delay curves are affected by the probe impedance to plasma (depending on ambient plasma conditions) and the WPT-Pre (AC) gain. In this figure, four typical cases are applied: (i) probe resistance of 10 MΩ with WPT-Pre (AC) H-gain, (ii) probe resistance of 100 MΩ with WPT-Pre (AC) H-gain, (iii) probe resistance of 10 MΩ with WPT-Pre (AC) low-gain, and (iv) probe resistance of 100 MΩ with WPT-Pre (AC) L-gain.

Figure 7 shows the noise level in the electric field spectral density for EWO-EFD, based on the electric noise floor of the preamplifier and the expected gain curves of WPT-Pre and EFD. This noise floor is based on case (i) of Fig. 6. Although the antenna length is relatively shorter than those in other geospace missions, this figure shows that PWE is capable of achieving its scientific objectives in the electric field measurement. However, note that the noise level in the frequency range lower than several Hz is determined by the stability of the probe potential to ambient plasma and not same with the value shown here. Both figures will be revised after the progress of antenna impedance analyses.

Onboard data processing and data pipeline on the ground

Electric field waveforms (512 Hz × 2) and potential waveforms (128 Hz × 4) produced by EFD are stored in the onboard memory on the PWE CPU#8 unit with a length of 200 s at maximum. They are processed and converted to the ground telemetry. The EFD telemetry has two categories, the continuous (medium) and bust (high) modes, as part of PWE's continuous- and burst-mode datasets.

The continuous-mode data are processed from the raw waveform and the potential data described in Table 2 and sent to the system data recorder after the compression. Then, all of these mode data are transferred to the

Table 2 Burst-mode data from the EFD system (raw data)

Data		Rate (bps)
Electric field: waveform	512 Hz × 16 bit × 2 ch (*u* and *v*) max: ~ ± 6.6 V (WPT-Pre input equivalent) [~ ± 220 mV/m]	16,384
Potential	128 Hz × 16 bit × 4 ch (*u1*, *u2*, *v1*, *v2*) max: ~ ± 100 V (WPT-Pre input equivalent)	8192
Total		24,576

Kasaba *et al. Earth, Planets and Space* (2017) 69:174
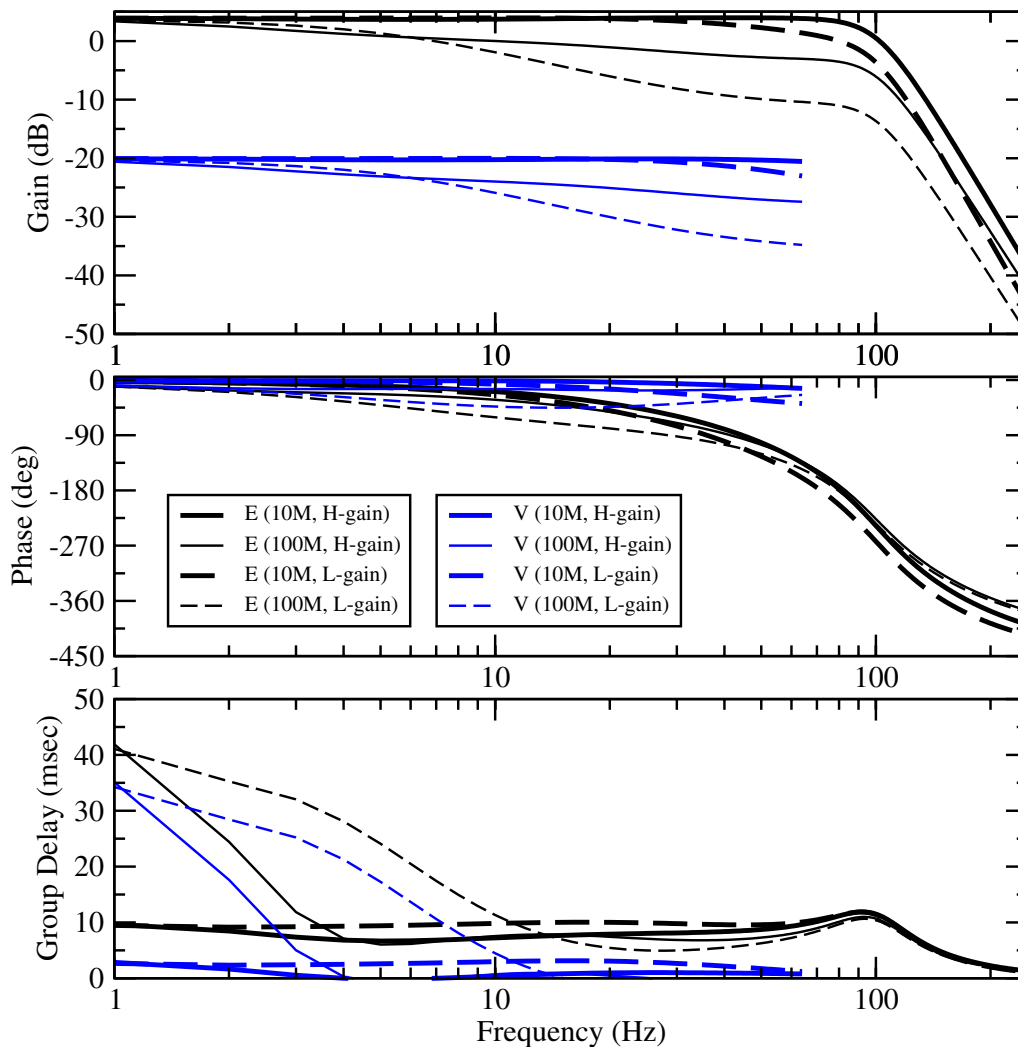
Page 10 of 18

Fig. 6 Assumed gain and phase characteristics of the WPT-Pre (DC) and EFD systems. From the top, gain, phase, and phase delay curves are shown in the frequency range of 1–256 Hz. Black lines indicate the differential electric field channels (E_u and E_v), which include the low-pass filter with a cutoff frequency of 100 Hz. Blue lines indicate the potential channels (V_{u1}, V_{u2}, V_{v1}, and V_{v2}), which directly reflect the characteristics of WPT-Pre (DC). The thick and thin lines indicate plasma resistance of ~ 10 and ~ 100 MΩ, respectively. Normal and dashed lines indicate the WPT-Pre (AC) H-gain and L-gain, respectively

ground. This mode contains (1) 2-ch electric field waveforms at 64 Hz (in Apoapsis mode, in $L > 4$) or 256 Hz (in Periapsis mode, $L < 4$), (2) 1-ch electric field spectrum at 1–232 Hz with 1-s resolution, and (3) 4-ch spacecraft potential at 8 Hz. When the electric field is larger than ~ 100 mV/m and the normal differential electric field output is close to be saturated, (4) 2-ch electric field at 128 Hz is also produced as the difference of the potential voltage between the U1/U2 ($E_{u\text{-}potdiff}$ component) and V1/V2 ($E_{v\text{-}potdiff}$ component) pairs. This mode has a dynamic range of ~ ± 3.3 V/m with a resolution of ~ 0.2 mV/m if the dipole antenna has an effective length of ~ 30 m. The definition of the EFD normal-mode data is summarized in Table 3.

The burst-mode data are the same as the raw electric field and potential data (Table 2). Since the amount of these data can increase, they are intermittently taken and stored in the Mission Data Processor (MDP) as part of the EWO-WFC burst data. In the Mission Data Recorder (MDR) of MDP, EFD has two long buffers with the size of 0.6 GB × 2, which can store the EFD data with a total length of ~ 80 h for × 2 [Sect. 5.2 and Table 5 in Matsuda et al. (2017)]. The burst data are partially transmitted to the Earth after selection by us, after checking the continuous-mode data. The burst mode contains (5) 2-ch electric field waveforms at 512 Hz and (6) 4-ch spacecraft potential at 128 Hz. The burst data have two categories: "chorus burst" mode (~ 8 s length) with WFC full
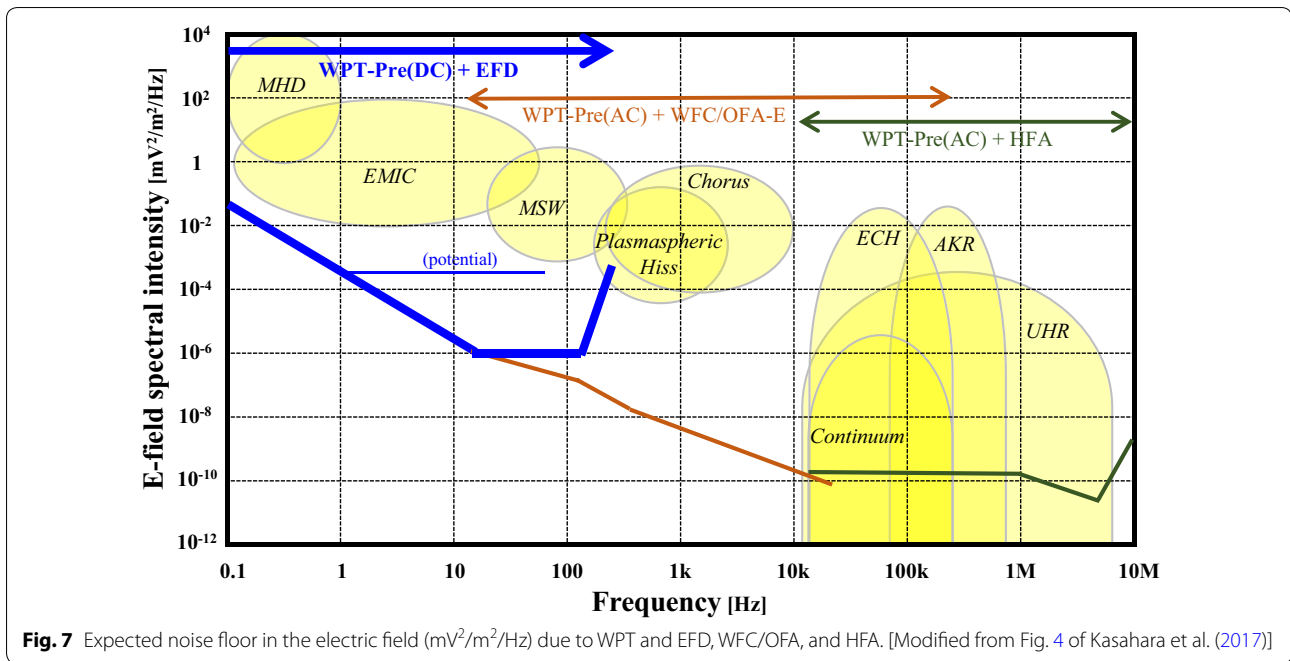
Kasaba *et al. Earth, Planets and Space* (2017) 69:174

Page 11 of 18

Fig. 7 Expected noise floor in the electric field (mV^2/m^2/Hz) due to WPT and EFD, WFC/OFA, and HFA. [Modified from Fig. 4 of Kasahara et al. (2017)]

Table 3 Continuous-mode data from the EFD system

Data		Rate (bps)
Electric field: waveform	64 Hz × 16 bit × 2 ch (*u* and *v*) [Apoapsis mode] or 256 Hz × 16 bit × 2 ch (*u* and *v*) [Periapsis mode]	2048 or 8192
Electric field: spectrum	1 Hz × 8 bit × 100 ch (1–224 Hz, *v* or *u*)	800
Potential	8 Hz × 8 bit × 4 ch (*u*1, *u*2, *v*1, *v*2)	256
Electric field: waveform	128 Hz × 16 bit × 2 ch (*u* and *v*) (when E-field waveform close to saturation)	(+ 4096)
Total [Apoapsis] [Periapsis] (when E-field close to saturation)		3104 or 9248 (+ 4096)

waveforms with 64 kHz sampled waveforms and "EMIC burst" mode (~ 180 s length) with WFC down-sampled waveforms at 1024 Hz. For EFD, both contain the same data.

For these telemetry definitions, EFD provides the electric field in the lower-frequency part as a counterpart of the magnetic field in a similar frequency range as that provided by MGF (sampling frequency: 256 Hz in Periapsis mode and 64 Hz in Apoapsis mode) and WFC/OFA-B low-frequency mode.

Initial evaluation status

WPT-S deployment operation

For the ISAS and JAXA spacecraft, there was a long gap in the development and deployment of wire antenna systems after the Geotail spacecraft was launched in 1992. Although we developed the wire antenna system as part of Plasma Wave Analyzer (Ono et al. 1998; Matsumoto et al. 1998) for the Nozomi (Planet-B) Mars orbiter

launched in 1998, we had no chance to try the deployment operation till its mission end (December 2004), because of the multiple bus system failures that occurred in December 1998 and April 2002. Therefore, the physical, mechanical, and operational establishments of the Arase WPT system are important not only for this mission but also for the BepiColombo mission to Mercury, in which the deployment operation of its wire probes (WPT and MEFISTO) will be remotely executed in 2025 after the Mercury orbit insertion (Kasaba et al. 2010).

The deployment operation of WPT-S was very carefully designed and smoothly executed by the support of JAXA, NEC Corporation (the manufacturer of Arase's Bus system), Mitsubishi Heavy Industries Ltd. (the manufacturer of Arase's Mission system, PWE-E, and WPT-Pre), and NIPPI Corporation (the manufacturer of WPT-S and MAST-WPT-E). Figure 8 shows the PWE data obtained during its deployment sequence. At each extension step, spikes in the spectrum were caused by the oscillation of

Kasaba *et al. Earth, Planets and Space* (2017) 69:174

Page 12 of 18

Kasaba *et al. Earth, Planets and Space* (2017) 69:174

Page 13 of 18
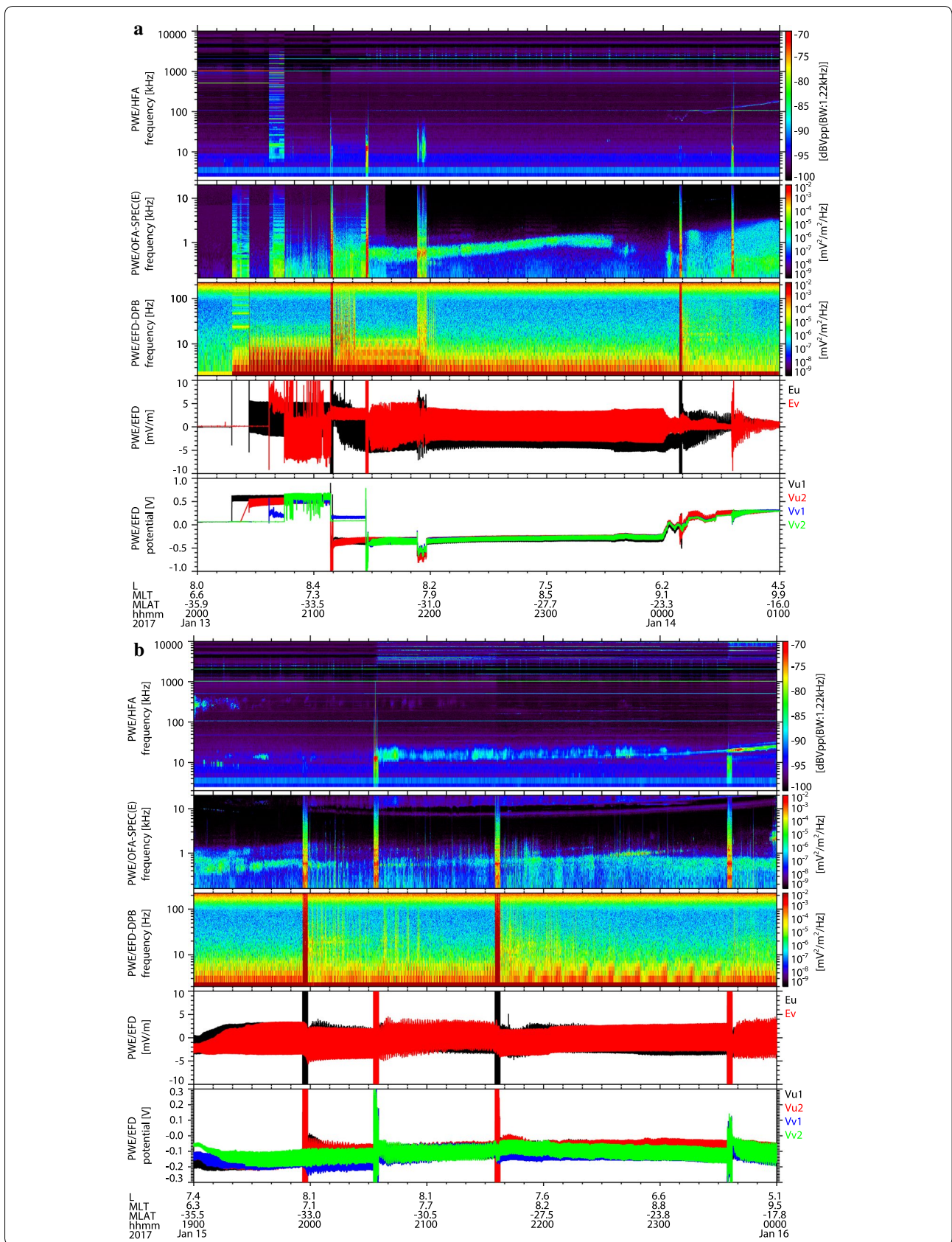
(See figure on previous page.)
Fig. 8 Electric field data of PWE before, during, and after the WPT-S deployment operation on **a** January 13–14, 2017, and **b** January 15, 2017. From the top, HFA spectrum (10 kHz to 10 MHz) (dt: 1 s), OFA-E spectrum (100 Hz to 20 kHz) (dt: 1 s), EFD E_v spectrum at 1–224 Hz (dt: 1 s), EFD 64 Hz electric field waveform of E_u (black) and E_v (red), and EFD 8 Hz spacecraft potential waveform of V_{u1} (black), V_{u2} (red), V_{v1} (blue), and V_{v2} (green) are shown. Although the antenna is not fully extended in these durations, the data are tentatively calibrated with the assumed effective antenna length of ∼ 30 m

antenna wires. At the latch release of WPT-S-U1 (20:18), WPT-S-U2 (20:26), WPT-S-V1 (20:36), and WPT-S-V2 (20:44) on January 13, 2017, each probe showed change in the potential from 0 V (grounded through the latching arm) to ∼ 0.5 V (floating), which shows the success of the latch-release actions of the spherical probes. All probes were still inside the spacecraft. From 21:08 and 21:26, WPT-S-U1/U2 and WPT-S-V1/V2 pairs were extended from 0 to 2.5 m. By the illumination on the probe by the Sun, the probe potential became positive due to the photoelectron emission. From 00:08 and 00:35 on January 14, 2017, additional extensions were executed for U1/U2 and V1/V2 pairs from 2.5 to 5.0 m. After the extensions, weak waves could be seen in the OFA and HFA frequency ranges. Since the critical operations were requested to maintain two ground-station tracking, we waited for a suitable timing and executed all extension sequences on January 15, 2017, from 19:56 and 20:32 for the 5- to 10-m extensions and from 21:35 and 23:34 for the final 10- to 15-m extensions.

After the full deployment, a strong electric filed induced by the Lorentz force (spacecraft velocity × background magnetic field) was detected just close to the periapsis. Since all antennas detected similar strength of this field with proper phase differences, we concluded that all WPT-S probes were successfully deployed with the same target length.

Stability, photoelectron emissivity, and antenna resistance of WPT-S

After the deployment, the amount of photoelectron emissions from the sphere and the conductive part of the wire should be stable enough for good electric field measurements. Since Arase's spin axis is set along the axis of the Sun with an angle of ∼ 15° (within 4–20°), the photoelectron emission from the spacecraft and the WPT wire booms is relatively stable. Although the wire boom can obtain dynamical turbulence associated with the fast temperature changes by the eclipse and the spin-axis changes by magnetic torquer operations, we confirm from the dynamical changes in the spacecraft that the maximum excited oscillation of the wire boom is ∼ 0.2° at a frequency of ∼ 40 s. Currently, we do not see any problem caused by this dynamical variation in the spacecraft, both in electric and in magnetic fields. We do not expect larger dynamical turbulences till the end of this mission.

From the relation between probe voltage and bias current, we can roughly estimate the photoelectron emissivity of each WPT-S sphere. This evaluation was executed on January 30, 2017, about 1 month after the launch and 2 weeks after the full deployment of WPT-S probes. Due to the saturation of probe potential caused by the excessive level of the bias current, the amount of photoelectrons is expected to be 60–100 nA (2.1–3.5 nA/cm^2) with slight difference between each probe.

The antenna resistance to ambient plasma was also initially evaluated by the bias sweep operations. From March, this evaluation has been executed in orbit once per month. The tentative result from March to June data is shown in Fig. 9, where the *X*-axis indicates the floating potential of the probe (positive: lower density) and the *Y*-axis indicates the resistance evaluated from bias current changes (dI_B) vs. probe potential changes (dV) around the initial bias current, I_b ∼ 19 nA. The evaluated antenna resistance is ∼ 10 MΩ in the higher density region inside of the plasmapause and ∼ 100 MΩ in the lower density region outside of the plasmapause. No large degradation was observed in these 4 months. This result is reflected in the gain-phase calibration curve (Fig. 9).

The antenna capacitance to the ambient plasma was also initially evaluated by the WPT-Pre (AC) calibration function (Kasahara et al. 2017; Matsuda et al. 2017). The test operation was executed on April 9, 2017, and its result is summarized in Table 4. The evaluated values of antenna capacity were 92–108 pF.

These parameters, their dependence on plasma conditions, and their variations will be investigated in more detail for the reflection of the calibration processes.

Initial data of EFD and the electric field data of PWE with WPT-S

Finally, the stack plot of PWE, including the EFD data and the electric field data of PWE with WPT-S, is shown, linked to other papers in this issue. Figure 10 shows the 1-day stack plot for April 9, 2017, corresponding to the same duration as that in Fig. 6 in Miyoshi et al. (2017a, b). The panels of HFA, OFA-E, and OFA-B spectra include the local electron gyro-frequency (black solid lines) and the half of the gyro-frequency (black dashed lines) derived from the MGF measurements. The HFA panel also shows the identified UHR frequency (white solid line), with the electron plasma frequency (white dashed
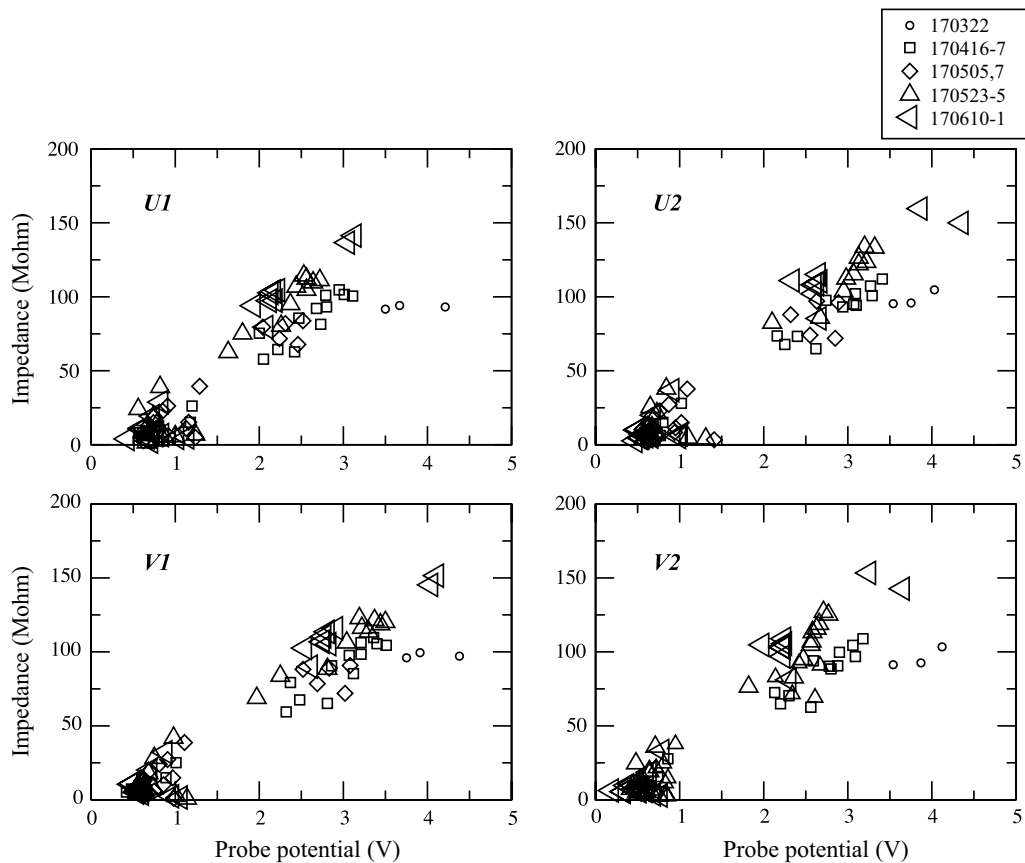
Kasaba *et al. Earth, Planets and Space* (2017) 69:174

Page 14 of 18

Fig. 9 Antenna resistance evaluated by the bias sweep operations during March–May 2017. X-axis indicates the floating probe potential (positive: lower density), and Y-axis indicates the estimated resistance. Each symbol shows the evaluated date by the bias current sweep operation: 170322, 170416-7, 170505 and 170507, 170523-5, and 170610-1
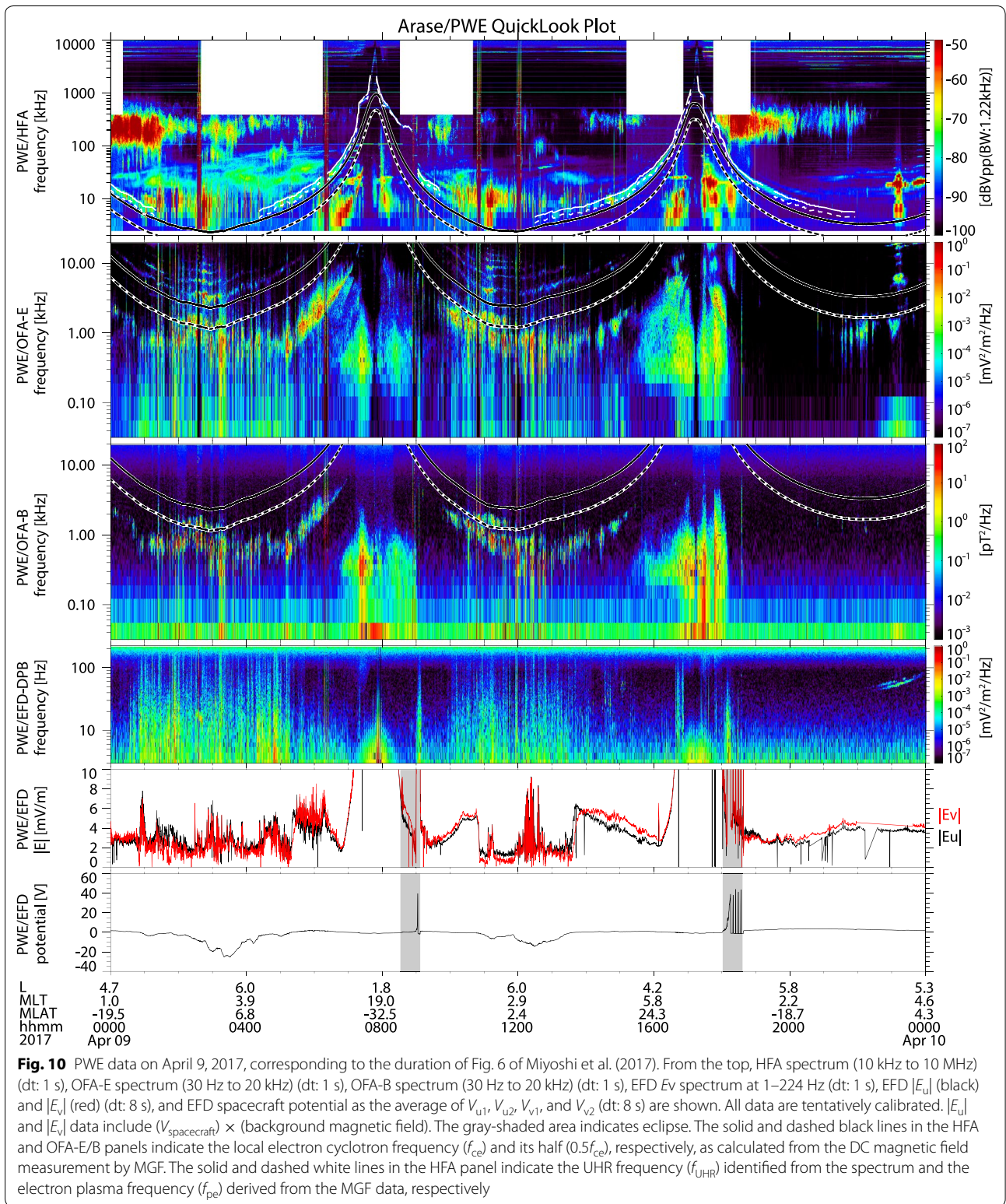
Table 4 Initial antenna capacity evaluation results

Date and time	Antenna capacity (pF)	Spacecraft potential (V)	f_{UHR} (MHz)
April 9, 2017 02-35-02	94	− 8.2	0.011
06-19-02	100	+ 1.4	0.26
08-55-00	104	+ 0.8	0.20
10-48-02	108	− 0.7	0.015
11-59-01	92	− 7.8	0.011

line) expected with the MGF data (Kumamoto et al. 2017). From EFD, the spectrum at 1–232 Hz (dt ~ 1 s), absolute electric field amplitude (black: $|E_u|$, red: $|E_v|$), and spacecraft potential as the average of V_{u1}, V_{u2}, V_{v1}, and V_{v2} are shown. Note that if the calibration assumption shown in Fig. 6 is not very far from the real one, this noise floor observed around 20 UT is similar to the observed one (e.g., the noise level observed on April 9 2017, in Fig. 10). Therefore, the noise floor in Fig. 7 is

similar to that observed in space at a frequency of 3 Hz and above.

The UHR observed in the HFA panel shows the electron density along Arase's orbit, whose apogee has an MLT of ~ 4 h (dawn side). Arase passed the periapsis (with the largest electron density (f_{UHR} ~ 7 MHz) and magnetic field (f_{ce} ~ 1 MHz) at the top side of the ionosphere) two times at ~ 8 h and 17 UT. Around the periapsis, the absolute electric field amplitude becomes much enhanced because the value plotted in this figure still includes the Lorenz field created by the spacecraft velocity with the magnetic field.

The waveform measurement capability of EFD at 64 Hz (Apoapsis mode) and 256 Hz (Periapsis mode) is requested from the mission design, in order to obtain an electric field waveform synchronized with the magnetic field waveform measured by MGF for the studies of the wave–particle interactions related to the low-frequency electromagnetic waves (e.g., EMIC waves). One example is seen around 23 UT, the banded emissions at ~ 70 Hz (magnetosonic mode waves). The waveforms of such

Fig. 10 PWE data on April 9, 2017, corresponding to the duration of Fig. 6 of Miyoshi et al. (2017). From the top, HFA spectrum (10 kHz to 10 MHz) (dt: 1 s), OFA-E spectrum (30 Hz to 20 kHz) (dt: 1 s), OFA-B spectrum (30 Hz to 20 kHz) (dt: 1 s), EFD E_v spectrum at 1–224 Hz (dt: 1 s), EFD $|E_u|$ (black) and $|E_v|$ (red) (dt: 8 s), and EFD spacecraft potential as the average of V_{u1}, V_{u2}, V_{v1}, and V_{v2} (dt: 8 s) are shown. All data are tentatively calibrated. $|E_u|$ and $|E_v|$ data include ($V_{spacecraft}$) × (background magnetic field). The gray-shaded area indicates eclipse. The solid and dashed black lines in the HFA and OFA-E/B panels indicate the local electron cyclotron frequency (f_{ce}) and its half (0.5f_{ce}), respectively, as calculated from the DC magnetic field measurement by MGF. The solid and dashed white lines in the HFA panel indicate the UHR frequency (f_{UHR}) identified from the spectrum and the electron plasma frequency (f_{pe}) derived from the MGF data, respectively

waves should be compared with their magnetic counterpart. Since the waveform and the spectrum with enough spectral resolution at a frequency of less than 200 Hz are

not provided by OFA-E, EFD is requested to provide this information. Although the sensitivity of EFD is limited by its lower gain and low-pass filter with a cutoff frequency

Kasaba *et al. Earth, Planets and Space* (2017) 69:174

Page 16 of 18

of 100 Hz, the capability is still effective if the wave amplitudes are strong enough.

During this interval, several substorm activities are observed from 00:00 UT to 14:00 UT, with several injections of electrons detected (Miyoshi et al. 2017). Such injections provide the free energy source to generate plasma waves, and outside of the plasmapause around the first and second apogees (∼ 3 h and ∼ 13 h UT), the chorus waves at a few hundred Hz to a few kHz are enhanced more than that observed in the second apogee (∼ 22 h UT). Such injections of hot electrons and subrelativistic electrons can clearly change the spacecraft potential to negative, < −10 V, as seen at ∼ 4 and ∼ 13 h UT. These magnetospheric disturbances also enhance the amplitude of the magnetospheric electric field more than the quiet status observed after the second perigee. After 17:00 UT, the spacecraft potential and wave spectrum also turn back to the quiet status because of nonsupply of free energy. The spacecraft potential only shows the several voltage variations linked to the ambient cold plasma density.

Ongoing evaluation work for the provision of public-open data (Level-2)

In the present paper, we introduced the specification and initial evaluation results of the WPT and EFD systems of the PWE instrument on the Arase satellite. Our system has been operated successfully with all PWE components and functions.

Currently, we are establishing the removal of the Lorentz electric field based on the accurate spacecraft velocity and magnetic field vector. We are also conducting a detailed calibration of the spacecraft potentials and electric field taken by the four WPT sensors with the EFD receiver. The qualities of these parameters are affected by the antenna resistance or the effective length of the WPT-S antennas, determined by the balance among photoelectrons, ambient inflow electrons, and electrons fed as the bias current. The photoelectron emissivity and secondary electron yields of WPT-S's sphere surfaces coated with TiAlN were originally be nonuniform before the launch. (No special cleanliness control was applied to the sphere surface.) They can be degraded after the launch, by a long exposure to atomic oxygen around periapsis and solar EUV emissions. We plan to evaluate the trend of the sphere surface characteristics, including our prelaunch evaluation results of the coating, and present it with the data of Arase's 1-year full operation, from April 2017 to March 2018. Antenna characteristics also vary with the ambient electron inflow, which depends on the ambient electron density and temperature and the injection of hot and energetic electrons. The following inter-instrument calibration is now being attempted: (1) spacecraft potential (PWE–EFD)—upper hybrid resonance frequency (PWE–HFA) for electron density calibration, (2) the ratio between electric field waveform (PWE–EFD) and magnetic field waveform (PWE–WFC-B + SCM or MGF) in the low-frequency electromagnetic waves for E/B calibration, (3) the DC electric field (PWE–EFD)—low-temperature particle velocity (LEP-i/e) for the electric field calibration (e.g., Kasaba et al. 2006) if the plasma velocity can be provided with enough quality, and (4) the evaluation of the possible effect from the plasma wakes created by the spacecraft motion (e.g., Miyake et al. 2015).

Arase does not have the capability to measure the electric field in parallel with the spacecraft spin axis, because of the limitation caused by the scale of the systems. However, Arase's spin axis, which is set nearly parallel to the Solar direction, enabled us to obtain probe potential data not contaminated by the shadow on the sphere probes caused by the spacecraft spin motion. We are trying to derive the well-calibrated potential and electric field data in collaboration with the staffs of Tohoku University (the WPT and EFD systems), Nagoya University (the ERG Science Center), and various other institutions. Furthermore, the EFD waveform will be calibrated in a similar way to WFC-E, for both intensity and phase as a function of frequency, which contains the EFD circuit impedance and the antenna impedance to ambient plasma. The data obtained after these calibrations will be released as Level-2 data from the ERG Science Center in Nagoya University.

In parallel, simultaneous data analyses with magnetic field and particles aboard the Arase spacecraft with the ground-based ionospheric radar (ionospheric density and electric fields), magnetometers, and aurora camera networks with multiple spacecraft observations are essential for the extraction of Arase's single-point observation to the variation and propagation of widespread electric and magnetic field structures (e.g., Takahashi et al. 2017). From the latter half of March 2017, Arase has started campaign observations with EISCAT and the PWING project (Shiokawa et al. 2017). We are providing partially calibrated data for these durations. The provision of the full calibrated data, including other durations, will also be initiated as soon as possible.

Author details
[1] Department of Geophysics, Tohoku University, Aoba-ku, Sendai, Miyagi 980-8578, Japan. [2] Department of Electronics and Informatics, Toyama Prefectural University, Imizu, Toyama 939-0398, Japan. [3] Graduate School of Natural Science and Technology, Kanazawa University, Kakuma-machi, Kanazawa 920-1192, Japan. [4] Research Institute for Sustainable Humanosphere (RISH), Kyoto University, Uji, Kyoto 611-0011, Japan. [5] Institute of Space-Earth Environmental Research, Nagoya University, Nagoya 464-8601, Aichi, Japan. [6] Tohoku Institute of Technology, Taihaku, Sendai 982-8577, Miyagi, Japan. [7] Department of Earth and Planetary Sciences, University of Tokyo, Bunkyo, Hongo 113-0033, Japan. [8] Department of Atmospheric and Oceanic Sciences, University of California Los Angeles, Los Angeles 90095, CA, USA. [9] Department of Electrical and Computer Engineering and Center for Space Physics, Boston University, Boston 02215, MA, USA. [10] Institute of Space and Astronautical Science, Japan Aerospace Exploration Agency, Chuo, Sagamihara 252-0222, Kanagawa, Japan. [11] Planetary Plasma and Atmospheric Research Center, Tohoku University, Aoba-ku, Sendai, Miyagi 980-8578, Japan. [12] Japan Aerospace Exploration Agency, Tsukuba 305-8505, Ibaraki, Japan.

Publisher's Note
Springer Nature remains neutral with regard to jurisdictional claims in published maps and institutional affiliations.

References
Bonnell JW, Mozer FS, Delory GT, Hull AJ, Ergun RE, Cully CM, Angelopoulos V, Harvey PR (2008) The electric field instrument (EFI) for THEMIS. Space Sci Rev 141:303–341. https://doi.org/10.1007/s11214-008-9469-2

Kasaba Y, Hayakawa H, Ishisaka K, Okada T, Matsuoka A, Mukai T, Takei Y (2006) Evaluation of DC electric field measurement by the double probe system aboard the Geotail spacecraft. Adv Space Res 37(3):604–609. https://doi.org/10.1016/j.asr.2005.05.006

Kasaba Y, Bougeret J-L, Blomberg LG, Kojima H, Yagitani S, Moncuquet M, Trotignon J-G, Chanteur G, Kumamoto A, Kasahara Y, Lichtenberger J, Omura Y, Ishisaka K, Matsumoto H (2010) The Plasma Wave Investigation (PWI) onboard the BepiColombo/MMO: first measurement of electric fields, electromagnetic waves, and radio waves around Mercury. Planet Space Sci 58:238–278. https://doi.org/10.1016/j.pss.2008.07.017

Kasahara Y, Kasaba Y, Kojima H, Yagitani S, Imachi T, Ishisaka K, Tsuchiya F, Kumamoto A (2016) Current status and planning of the Plasma Wave Experiment (PWE) onboard the ERG satellite, In: 2016 URSI Asia-Pacific radio science conference. https://doi.org/10.1109/ursiap-rasc.2016.7601229

Kasahara Y, Kasaba Y, Kojima H, Yagitani S, Ishisaka K, Kumamoto A, Tsuchiya F, Ozaki M, Matsuda S, Imachi T, Miyoshi Y, Hikishima M, Katoh Y, Ota M, Matsuoka A, Shinohara I (2017) The Plasma Wave Experiment (PWE) on board the Arase spacecraft. Earth Planets Space. http://doi.org/10.1186/s40623-017-0759-3

Kumamoto A, Tsuchiya F, Kasahara F, Kasaba Y, Kojima H, Yagitani S, Ishisaka K, Imachi T, Ozaki M, Matsuda S, Shoji M, Matsuoka A, Katoh Y, Miyoshi Y, Obara T (2017) High Frequency Analyzer (HFA) of Plasma Wave Experiment (PWE) onboard the ARASE spacecraft, Earth Planets Space, this issue

Matsuda S, Kasahara Y, Kojima H, Kasaba Y, Yagitani S, Ozaki M, Imachi T, Ishisaka K, Kumamoto A, Tsuchiya F, Ota M, Kurita S, Miyoshi Y, Hikishima M, Matsuoka A, Shinohara I (2017) Onboard software of Plasma Wave Experiment aboard Arase: instrument management and signal processing of waveform capture/onboard frequency analyzer. Earth Planets Space. http://doi.org/10.1186/s40623-017-0758-4

Matsumoto H, Nagano I, Anderson RR, Kojima H, Hashimoto K, Tsutsui M, Okada T, Kimura I, Omura Y, Okada M (1994) Plasma wave observations with Geotail spacecraft. J Geomagn Geoelectr 46:59–95. https://doi.org/10.5636/jgg.46.59

Matsumoto H, Okada T, Hashimoto K, Nagano I, Yagitani S, Tsutsui M, Kasaba Y, Tsuruda K, Hayakawa H, Matsuoka A, Watanabe S, Ueda H, Kasahara Y, Omura Y, Ishisaka K, Imachi T, Tateno Y (1998) Low Frequency plasma wave Analyzer (LFA) onboard the PLANET-B spacecraft. Earth Planets Space 50(3):223–228. https://doi.org/10.1186/BF03352107

Miyake Y, Nishimura J, Kasaba Y (2015) Asymmetric electrostatic environment around spacecraft in weakly streaming plasmas. J Geophys Res Space Phys. https://doi.org/10.1002/2015JA021064

Miyoshi Y, Ono T, Takashima T, Asamura K, Hirahara M, Kasaba Y, Matsuoka A., Kojima H., Shiokawa K., Seki K., Fujimoto M., Nagatsuma T., Cheng C.Z., Kazama Y, Kasahara S, Mitani T, Matsumoto H, Higashio N, Kumamoto A, Yagitani S, Kasahara Y, Ishisaka K, Blomberg L, Fujimoto M, Katoh Y, Ebihara

Kasaba *et al. Earth, Planets and Space* (2017) 69:174

Page 18 of 18

Y, Omura Y, Nose M, Hori T, Miyashita Y, Tanaka Y, Segawa T, ERG working group (2012) The Energization and Radiation in Geospace (ERG) Project. In: Summers D, Mann IR, Baker DN, Schulz M (eds.) Dynamics of the earth's radiation belts and inner magnetosphere, Geophys Monogr Ser 199:103–116. https://doi.org/10.1029/2012bk001304

Miyoshi Y, Kasaba Y, Shinohara I, Takashima T, Asamura K, Matsumoto H, Higashio N, Mitani T, Kasahara S, Yokota S, Wang S, Kazama Y, Kasahara Y, Yagitani S, Matsuoka A, Kojima H, Katoh Y, Shiokawa K, Seki K, Fujimoto M, Ono T, ERG project group (2017a) Geospace exploration project: arase (ERG). J Phys Conf Ser 869(1):012095. https://doi.org/10.1088/1742-6596/869/1/012095

Miyoshi Y, Shinohara I, Takashima T, Asamura K, Higashio N, Mitani T, Kasahara S, Yokota S, Kazama Y, Wang S.-Y, Ho P, Kasahara Y, Kasaba Y, Yagitani S, Matsuoka A, Kojima H, Katoh Y, Shiokawa K, Seki K (2017b) Geospace Exploration Project ERG: overview, Earth Planets Space, this issue

Ono T, Oya H, Morioka A, Kumamoto A, Kobayashi K, Obara T, Nakagawa T (1998) Plasma Waves and Sounder (PWS) experiment onboard the Planet-B Mars orbiter. Earth Planets Space 50:213–221. https://doi.org/10.1186/BF03352106

Okano TS, Michizono S, Saito Y, Tumiran Yamano Y, Kobayashi S (2006) Photo-electron emission of TiN-coated alumina excited by ultraviolet light. In: 2006 International symposium on discharges and electrical insulation in vacuum, Matsue, pp 120–123. https://doi.org/10.1109/deiv.2006.357246

Ozaki M, Yagitani S, Kojima H, Kasahara Y, Kasaba Y, Matsuoka A, Sasaki T, Yumoto T (2017) Magnetic Search Coil (MSC) of Plasma Wave Experiment (PWE) aboard the Arase (ERG) satellite, Earth Planets Space, this issue

Pedersen A, Mozer F, Gustafsson G (1998) Electric field measurements in a tenuous plasma with spherical double probes, in measurement techniques in space plasmas: fields. Geophys Monogr Ser 103:1–12, Pfaff RF, Borovsky JE, Young DT (eds) AGU, Washington, DC

Shiokawa K, Kato Y, Hamaguchi Y, Yamamoto Y, Adachi T, Ozaki M, Oyama S-I, Nose M, Nagatsuma T, Tanaka Y, Otsuka Y, Miyoshi Y, Kataoka R, Takagi Y, Takeshita Y, Shinbori A, Kurita S, Hori T, Nishitani N, Shinohara I, Tsuchiya F, Obara Y, Suzuki S, Takahashi N, Seki K, Kadokura A, Hosokawa K, Ogawa Y, Connors M, Ruohoniemi JM, Engebretoson M, Turunen E, Ulich T, Manninen J, Raita T, Kero A, Oksanen A, Back M, Kauristie K, Mattanen J, Baishev D, Kurkin V, Oinats A, Pashinin A, Vasilyev R, Rakhmatulin R, Bristow W, Karjala M (2017) Ground-based instruments of the PWING project to investigate dynamics of the inner magnetosphere at subauroral latitudes as a part of the ERG-ground coordinated observation network. Earth Planets Space 69:160. http://doi.org/10.1186/s40623-017-0745-9

Takahashi N, Kasaba Y, Nishimura Y, Shinbori A, Kikuchi T, Hori T, Ebihara Y, Nishitani N (2017) Propagation and evolution of electric fields associated with solar wind pressure pulses based on spacecraft and ground-based observations. J Geophys Res Space Phys. https://doi.org/10.1002/2017JA023990

Torbert RB, Russell CT, Magnes W, Ergun RE, Lindqvist P-A, Le Contel O, Vaith H, Macri J, Myers S, Rau D, Needell J, King B, Granoff M, Chutter M, Dors I, Olsson G, Khotyaintsev YV, Eriksson A, Kletzing CA, Bounds S, Anderson B, Baumjohann W, Steller M, Bromund K, Le G, Nakamura R, Strangeway RJ, Leinweber HK, Tucker S, Westfall J, Fischer D, Plaschke F, Porter J, Lappalainen K (2016) The FIELDS instrument suite on MMS: scientific objectives, measurements, and data products. Space Sci Rev 199(1–4):105–135. https://doi.org/10.1007/s11214-014-0109-8

Tsuruda K, Hayakawa H, Nakamura M, Okada T, Matsuoka A, Mozer FS, Schmidt R (1994) Electric field measurements on the GEOTAIL satellite. J Geomagn Geoelectr 46:693–711. https://doi.org/10.5636/jgg.46.693

Wygant JR et al (2013) The electric field and waves (EFW) instruments on the radiation belt storm probes mission. Space Sci Rev 179:183–220. https://doi.org/10.1007/s1124-013-0013-7